# Title: Material selection and detailed design of optical windows under high loads

Journal: Materials & Design; http://www.journals.elsevier.com/materials-and-design/

Article type: Technical report


| | | | |
|---|---|---|---|
| 1* | Balazs Ihracska | University of Hertfordshire, School of Engineering and Technology, College Lane Hatfield, Hertfordshire AL10 9AB, UK | a.b.ihracska@herts.ac.uk |
| 2 | Roy James Crookes | School of Engineering and Materials Science, Queen Mary University of London, London E1 4NS, UK | r.j.crookes@qmul.ac.uk |
| 3 | Diogo Montalvão | Department of Design and Engineering, Faculty of Science and Technology, Bournemouth University, Talbot Campus, Fern Barrow, Poole, Dorset BH12 5BB, UK | dmontalvao@bournemouth.ac.uk |
| 4 | Mohammad Reza Herfatmanesh | University of Hertfordshire, School of Engineering and Technology, College Lane Hatfield, Hertfordshire AL10 9AB, UK | m.r.herfatmanesh@herts.ac.uk |
| 5 | Zhijun Peng | University of Hertfordshire, School of Engineering and Technology, College Lane Hatfield, Hertfordshire AL10 9AB, UK | z.peng2@herts.ac.uk |
| 6 | Shahid Imran | Department of Mechanical Engineering (KSK Campus), University of Engineering and Technology, Lahore, Pakistan | shahidimran512@hotmail.com |
| 7 | Theodosios Korakianitis | Parks College of Engineering, Aviation and Technology, Saint Louis University, St. Louis, MO 63103, USA | talexander@slu.edu |

*corresponding author

## Abstract

In this study, the design aspects of optically accessible pressure vessels are investigated via a case study of a High Pressure Combustor experimental rig. The rig was designed to take optical measurements of combustion, simulating the conditions found in internal combustion engines and turbines. Although, it is not new to equip chambers and reactors with sight windows, important aspects of design and relevant information regarding optical access is missing or are insufficiently explored or not readily accessible in the existing literature. A comprehensive review of requirements for optical access to such high-pressure, high-temperature systems has been conducted. It is shown in a readily-navigable format as function of application and precision, with data and technical correlations hitherto not found in a 'user-friendly' style. The material selection procedure is detailed and supported by a complete comparison of optical materials and relevant properties. The review revealed a significant inconsistency in mechanical properties claimed in the literature for optical materials. As a response to this, increased safety factor values are suggested as function of level of uncertainties and effects of failure, typically three to four times higher than the industrial standard. Moreover, newly developed equations are presented linking performance analysis to the design criteria.

Keywords:

- Optically-accessible reactor,
- Optical engine,
- Pressure vessel;
- Sapphire,
- Window design,
- Combustion

# 1 Introduction to the High Pressure Combustor (HPC) and the need for optical development

Over the past two decades, concerns about global warming and the depletion of the ozone layer have driven researchers to find better alternatives to the high energy consumption demand [1-4]. With the combustion of fossil fuel and the subsequent production of carbon dioxide being accounted for as the main contributor to the current release of greenhouse gases to the atmosphere [5], and taking into consideration that a solution to the current energy supply problems is yet distant, improvements in the understanding of the chemical reaction and flame-propagation processes and reduction the emissions of these engine-fuel combinations should be implemented as a short term solution [6-8].

The HPC was developed to address research topics in combustion science. Its unique design makes it a versatile tool to model and test the working, at real-life conditions of industrial furnaces, external and internal combustion engines and gas turbines. It can be set up to test steady combustion up to 60 bar for 30 minutes. It can accept virtually any combustible substance with a high accuracy of air-fuel ratio and a control of residence time. Moreover, the flow pattern can be set to either plug or swirl. The high-pressure air (variable up to 60 bar) is delivered to the chamber via a number of safety instruments from a large air receiver – which is charged by a three-stage piston pump. The air arriving to the combustion chamber is dried, and its flow and pressure is set by a computer-controlled valve system. The fuel is injected into the chamber by interchangeable injectors; the fuel flow pattern, supply pressure and volume flow is variable. The actual combustion chamber is not a single-piece vessel but rather an assembly of several sections. Therefore, the length of the chamber – and hence, the residence time of reactants – can be varied depending on the application. The sections were designed with numerous radial access points so that reaching any point inside the combustor for sampling would be possible; see Figure 1 for a schematic of the experimental rig. The initial ignition is provided by a high-energy spark. At the end of the process, the burned mixture leaves the chamber via a special plunger valve that is capable of withstanding the high temperature and pressure. A detailed description of the HPC facility can be found in [9-11].

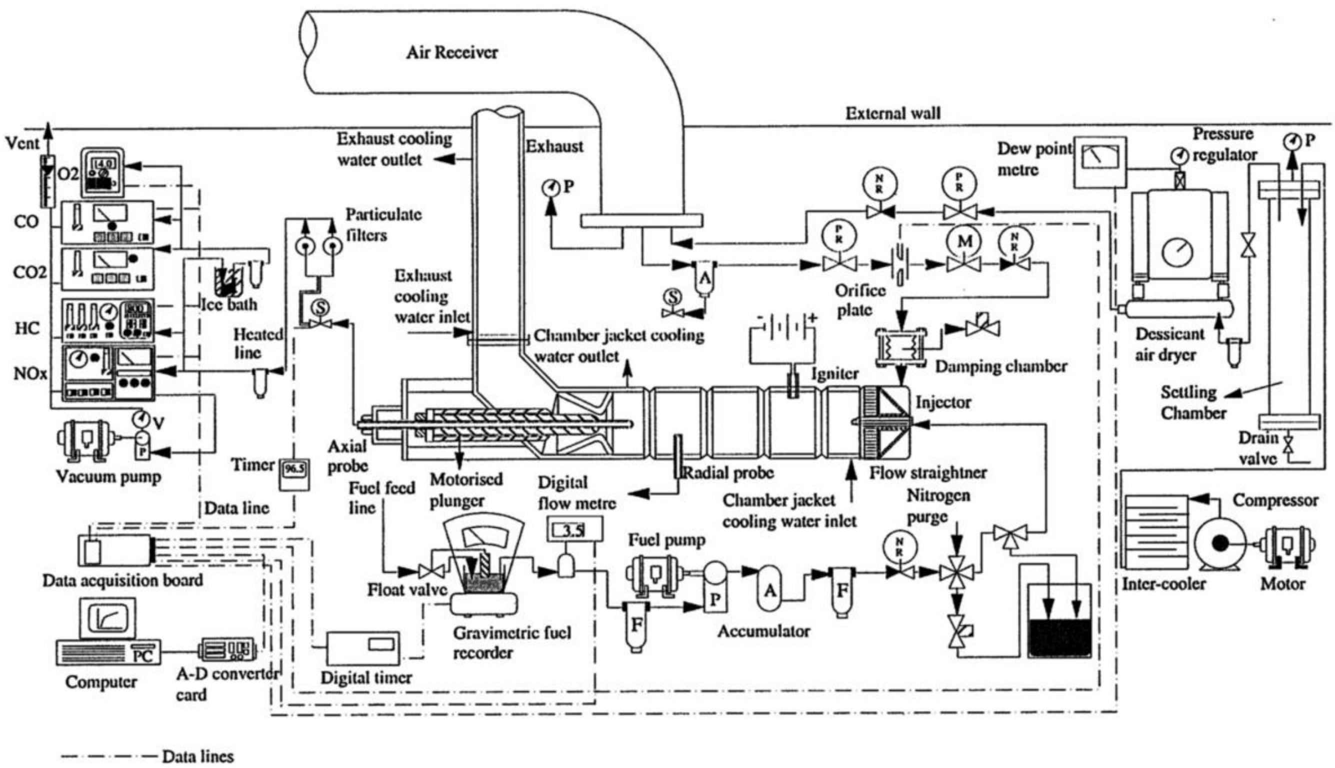


**Figure 1. Schematic drawing of the experimental rig, adapted from [10].**

The HPC has supplied the combustion research community with vital information. Using thermocouples and sample probes, its current capabilities have been fully utilised. New developments were needed to keep the rig up-to-date. In the last 15 years or so, the optical- and laser-based measurements became the most important tools to investigate combustion details and results of these methods published elsewhere [12-14]. These methods have a fast response time and do not require actual physical contact with the flames. It was essential to equip the HPC with optical access in order to keep the research work current and on-going.

# 2 Current contribution

The design methods and procedures of industrial pressure vessels are well-documented, with comparisons of methods and standards available for industrial applications [15-25]. These provide good guidelines even for an unconventional design task, but of course they do not provide comprehensive data for all possible cases.

In general, the available literature lacks data regarding optical access to pressurised vessels. Information on design practices and material properties are scattered in the literature, being hard to find and often inconsistent. In this work, novel complementary material is provided for the design of chambers and reactors that require the equipment of sight windows on them. As a result of extensive review, the properties of practical optical materials were collected and presented together in graphs and tables, allowing for direct comparison. The details of special design practices regarding transparent parts are discussed, and the available data on existing design solutions is collected and shown. Some complementary material is added to the basic equations and relations in Statics. Moreover, there are papers examining design procedures [26], but to the authors' knowledge this is the first detailed design study on optically accessible pressure vessels (fixed volume or internal combustion optical engine) where the real-life application of the collected data is shown. Structural analysis of optical material window is shown and its effects to practical design.

# 3 The optical access: review of material and their properties; practical solutions; mechanical and optical performance

## 3.1 Optical materials: mechanical, optical and chemical properties

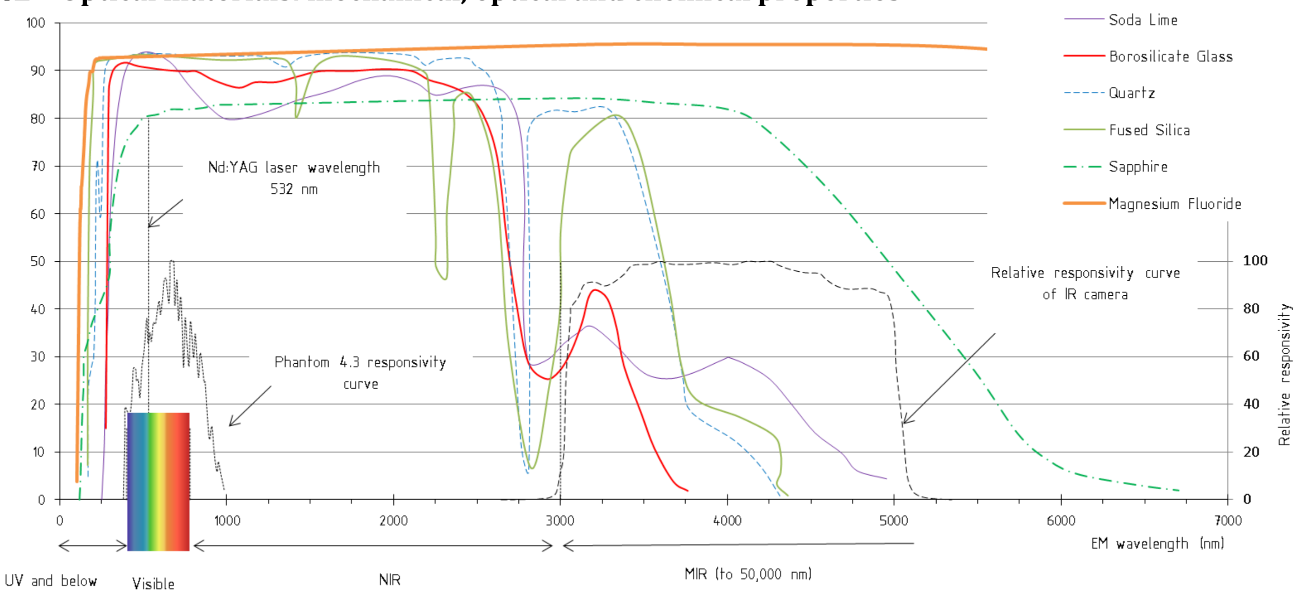


**Figure 2 Transmittance of the reviewed optical materials; relative responsivity and wavelength of interest are also shown (for Design requirements section).**

There are a large number of materials that can be considered for sight windows on pressure vessels, from ordinary plastics to exotic ceramics. In this work, only the most common and most practical optical materials were chosen for comparison.

The underlying design criteria for selecting the optimal optical material type are: useful transmittance range, operating temperature and mechanical load. In Table 1, only high-operating-temperature materials are listed. It is important to note there are other choices available for specialised tasks, such as silicon or germanium, but their availability is limited and they are costlier. In low-temperature environments, plastics like acrylic and polycarbonate can be used. During design, it is essential to consider the working temperature and obtain a good estimate of it from simulations or experiments.

Although unusual in mechanical engineering, it is important to choose the right material for the required electromagnetic band. It is also vital to consider the ratio of the electromagnetic energy falling on a body to that transmitted through it. This ratio is called the transmittance of the material [27]. Transmittance values for each wavelength vary significantly among material. For example, a larger selection of materials can be considered if the investigated radiation is in the visible or in the near infra-red (NIR) regions. Due to the availability of a wider range of materials, the implication is that sight windows for high speed imaging or laser-aided measurements can be designed more easily, and more complex shapes with larger dimensions are therefore possible. Choosing an optimal material is more complex when longer wavelengths have to be captured for both spectroscopy and thermal imaging. For wavelengths over 2500 nm, the transmittance curves start fluctuating or becoming discontinuous. If this, then, is the electromagnetic wave band region of interest, careful planning will be needed to select the right material type. The transmittance of common optical materials for wavelengths under 200-250 nm falls rapidly. Yet, it is an important region in combustion science as some radicals have their peak emissivity in this electromagnetic band. Researchers and designers are practically left with fused silica and a number of fluorides ($MgF_2$, $CaF_2$, $BaF_2$) to use. Figure 2 shows the transmittance curves of selected materials.

Once the material candidates are shortlisted by wavelength transmittance, the more conventional design process follows this when further mechanical, thermal and chemical resistance properties are of interest.

Finally, the cost analysis needs to be taken into account when the material type providing the optimal solution is chosen.

Table 1 summarises some of the most related properties of a selection of practical optical materials. As expected, all of the listed properties are functions of temperature, size and shape, exact composition, heat treatment, surface finish, and other manufacturing processes. It is important to note that there are significant differences (10-15%) between the claimed values by different manufacturers and textbooks.

**Table 1. Optical material properties**

| | Unit | Soda Lime Glass | Borosilicate | Quartz | Fused Silica | Sapphire | Magnesium Fluoride |
|---|---|---|---|---|---|---|---|
| General | | | | | | | |
| Chemical Formula, Composition | (weight %) | $SiO_2$:74, $Na_2O$:15, CaO:5, others | $SiO_2$:80+, $B_2O_3$:7-13%, $Na_2O$, others | $SiO_2$:99 | SiO2:99 | $Al_2O_3$:99 | $MgF_2$:99 |
| Density | ($g/cm^3$) | 2.2-2.52 | 2.2-2.4 | 2.2 | 2.2 | 3.98 | 3.18 |
| Optical | | | | | | | |
| Useful Transmission | (nm) | 320-2300 | 325-2100 | 200-2400 | 180-2200 | 150-5000 | 110-7500 |
| Refractive index (588 nm) | - | 1.52 | 1.47 | 1.46 | 1.46 | 1.76 | 1.38 |
| Mechanical [I] | | | | | | | 0 |
| Young's Modulus | (GPa) | 72 | 64 | 73 | 73 | 335 | 138 |
| Tensile Strength | (MPa) | 41 | 27-62 | 50 | 50 | 275 [II] | 140 |
| Hardness, Vickers | - | 550 | 520-580 | 1000-1200 | 1000-1200 | 1940 | 400 |
| Poisson's ratio | - | 0.23 | 0.21 | 0.17 | 0.17 | 0.25 | 0.27 |
| Weibull variability of strength | - | 6 [III] | 30 [IV] | 8.82 [V] | 10.2 [VI] | 5 | 5 |
| Weibull stress | (MPa) | 129 [III] | 71 [IV] | 115 [V] | 180 [VI] | 485 | 96 |
| Thermal | | | | | | | |
| Softening Point | (°C) | 1450 | 800-850 | 1730 | 1600 | 2300 [VII] | 1255 |
| Max. Continuous Operating Temperature | (°C) | 260 | 280-350 | 950-1150 | 950-1100 | 1200 | 500 |
| Thermal Conductivity at 300 K | (W/mK) | 0.96 | 1.1-1.2 | 1.38 | 1.38 | 27.21 | 11.6 |
| Coefficient of Expansion | ($10^{-6}$/K) | 3.5-9 | 3.25-4 | 0.55 | 0.55 | 8.4 | 8.9 |

properties perpendicular to optical axis

materials are birefringent for exact refractive indexes see references

[I] mechanical and optical properties are dependent on fabrication method and surface finish; [II] fractural strength; [III] Kimble R-6; [IV] BK-7; [V] standard polish; [VI] "super polish"; [VII] melting point

Soda lime glass is the common glass type that can be found everywhere. It is mass-manufactured by floating the hot raw material on a bed of molten tin. It is the least expensive material of all, and being softer than other glasses, it is easy to make a complex part out of it. It is a hard material with good scratch resistance, but is significantly softer than other glasses or sapphire. It is not resistant to many chemicals, and its higher coefficient of expansion makes it sensitive to uneven temperature distribution [28-32].

Borosilicate glass is 2-3 times more expensive than soda lime glass but still considerably less expensive than fused quartz or silica. It has the same easy manufacturing properties as soda lime but usually has a lower thermal expansion coefficient, hence making it more resistant to thermal shock. Leaching can occur but it is more resistant to chemicals [28-31, 33, 34].

Fused quartz and silica have very similar properties as they have an almost identical composition. The main difference between them is in the amount of contamination caused by the different manufacturing processes. Quartz is made from melted and cleansed naturally occurring quartz sand with larger amount of contamination in the product, while fused silica is a pure version of quartz synthesised from various gases. However, their mechanical and electrical properties are identical. The only contrasting (and significant) advantage is that, silica has an excellent transmittance in the ultra violet

(UV) region. This property makes it unique among silicon oxides. A major advantage of quartz and silica, when compared to cheaper glasses, is their increased stability. Their mechanical properties are significantly less sensitive to temperature changes than borosilicate or float glasses. For instance, for a borosilicate, the linear thermal expansion at 500 °C increases its ambient value a few hundred times; silica, however, faces an increase of about 40 times and then stays constant with further increase of the temperature. This makes the evaluation of thermal stresses a lot easier when implementing quartz and silica. Nevertheless, their excellent properties come at a price: the material cost is significantly higher than the aforementioned glasses and their higher temperature resistance makes fabrication more complex. They have a reasonably good resistance to chemicals but break down with some caustics, fluorinated acids and plasmas [28-31, 33-36].

Sapphire is a single crystal and a very versatile material. It is the second hardest material on Earth, which makes it best choice of material whenever wear and abrasion are the main constraints. Its high mechanical strength and modulus of elasticity provides good resistance against impacts. It is virtually impervious to all corrosive materials and its thermal stability outperforms all other optical materials. Yet, sapphire raw material is not significantly more expensive than fused silica. On the other hand, its extreme hardness and a high melting point make the manufacturing process challenging and costly. In conclusion, sapphire is not suitable for large windows and for complex shapes [37-43].

Magnesium fluoride is an excellent material choice for application in the UV bandwidth (the cheaper $CaF_2$ has similar properties but with slightly reduced useful transmittance range). Larger size crystals can be grown, and it is possible to machine it with standard diamond tools as this material can be polished well. Thus, complex shapes and geometries can be achieved. It has a wide range of transmissivity but it is not as wear-resistant as the other materials, and its surface will degrade in a humid environment at elevated temperatures (over 500 °C) [33, 39, 44-46].

## 3.2 Mounting methods

There are a number of different ways to hold the optical element within an optical apparatus. A particular mounting method can be selected considering the geometric constraints, the sealing requirements, position accuracy, the orientation of optical axis, stress and the deformation caused by pressure difference, and birefringence. In this paper, sight optics is investigated only; their mounts are less complex than lenses that need more degrees of freedom.

### 3.2.1 Optical element kept in place by a guided clamp

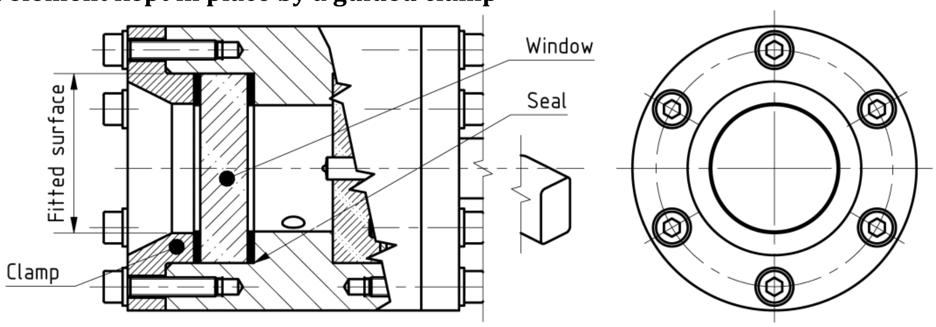


**Figure 3. Fixed volume combustion chamber with circular window that is positioned by a guided clamp [47].**

Figure 1 shows the usual clamping method where the retainer is fitted and guided in the directon of the displacement of the window. The radial position of the retainer is fully defined by the contact forces. The advantage of this solution is the simple tensile load on fixing bolts, and simplified dismantling and re-assembly. Details of loaded bolted joints can be found in the literature [48]. The disadvantage here is that the larger the size in the direction of optical axis, the more complex its design and manufacturing turns out to be [49].

### 3.2.2 Optical element kept in place by a free sitting clamp

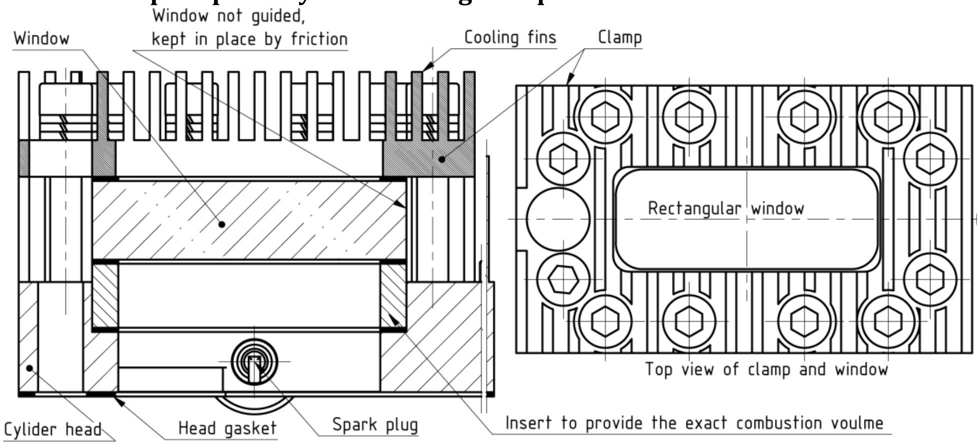


**Figure 4. Four-stroke optical engine, the rectangular window is sandwiched by the clamp and soft gaskets [6, 7].**

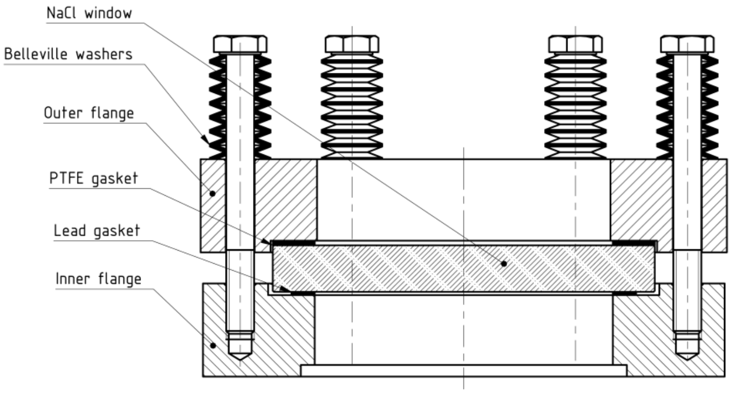


**Figure 5. Special sodium chloride free sitting window for a high-temperature, high pressure difference, IR spectra [50]**

The simplest design solution is illustrated in Figure 4 and Figure 5. The clamp is not guided but constrained by contact in one axis and constrained by friction along the other two axes; its position is defined by fixing bolts. Its advantages are: a simpler design, easier to manufacture, smaller in size along the optical axis, and that its position along the optical axis can easily be varied. Its disadvantage is that a greater amount of mechanical (bending) load on bolts is required; since the window can freely move, bringing the assembly together can also be problematic.

### 3.2.3 Adhesives

Fixing an optical element in a carrier frame using adhesives, as indicated in Figure 6 is a convenient solution for lower pressure and temperature environments. In both cases, the window sits against a shoulder which provides an accurate positioning. All mechanical loads rising from the pressure differential are taken by the adhesive. In the second case, the adhesive acts as a sealant and retainer; only, the stress is induced, but the pressure difference is taken by the shoulder on the frame cell. The main advantage of this solution is the modest space requirement. Its only disadvantage is that the performance of the assembly is proportionately dependent on the properties of the adhesive, which are usually limited.

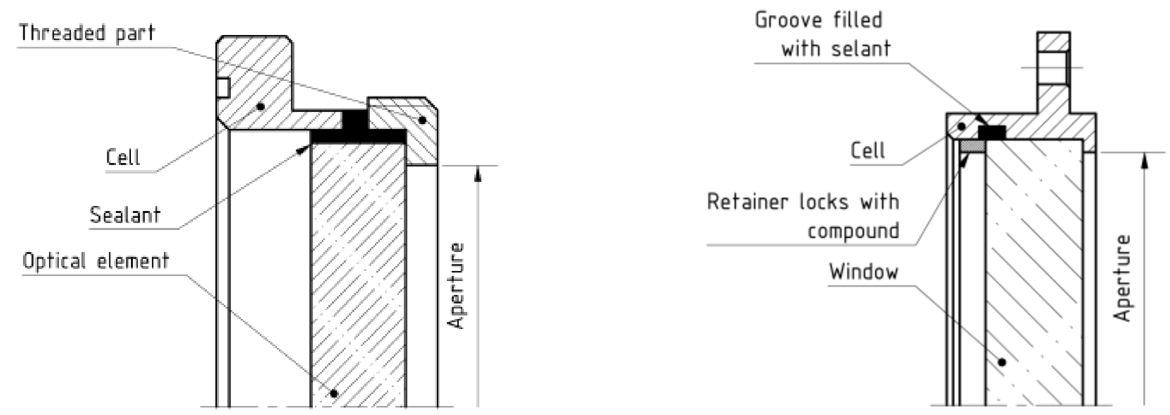


a,

b,

**Figure 6. a, Using adhesives for a low pressure application [51]; b, Using adhesives for a moderate pressure application [52].**

### 3.2.4 Fitted inside the shell of the vessel

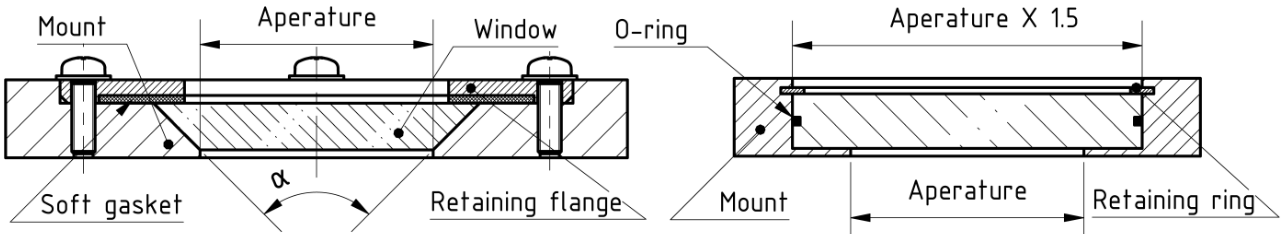


**Figure 7. Window integrated in the vessel body [53, 54].**

The optical element can be fitted inside the housing, a typical application area is the deep submergance vehicles, Figure 7. There is no need for bolts as the major load-bearing element. Its advantage is that this setup can take large pressure differences, while the vessel geometry can also be made more simply. Its disadvantage is that the window can only be dismantled from the pressurised side, more complex window geometry required.

## 3.3 Mechanical performance

### 3.3.1 Allowable or design stress in the optical element, safety factor

The estimation of the allowable or design stress is among the most important and sometimes challenging tasks, especially at elevated temperatures [23-25, 55-57]. The data of mechanical properties can be found in the literature for the more common materials; however, there often is no consistency in the given values. It becomes even more difficult to find information when practical issues are being considered, such as the effects of temperature, humidity, manufacturing technology, surface finish, and loading rate. Pressure vessel codes provide suggestions for high strength alloys which can then be taken as a first guidance for optical materials. According to BS EN 13445-3 [56] and ASME Boiler and Pressure Vessel Code Section VIII [57], the design stress should be calculated as:

(EN) $$\sigma_{des} = \min\left(\frac{R_{p0,2/T}}{SF}\, ;\, \frac{R_m/20}{SF}\right) = \min\left(\frac{R_{p0,2/T}}{1,5}\, ;\, \frac{R_m/20}{2,4}\right) \quad (1)$$

(ASME) $$\sigma_{des} = \min\left(\frac{R_{p0,2/T}}{SF}\, ;\, \frac{R_m/20}{SF}\right) = \min\left(\frac{R_{p0,2/T}}{1,5}\, ;\, \frac{R_m/20}{2,14}\right) \quad (2)$$

where, $\sigma_{des}$ is the allowable design stress; $SF$ is the safety factor; $R_{p0,2/t}$ is the 0,2% proof strength at T temperature; $R_m$ is the tensile strength at 20 °C [58]. As optical materials discussed in this work have brittle characteristics, it is only the safety factors that are associated with the tensile strength that are applicable. It is suggested that the safety factor for optical design should always exceed 2. The general value for a well-designed system is around 3, when failure is not expected to cause major damage. When there is more uncertainty in the design, the usual and conservative safety factor value is 4. The value can be as high as 5 for non-optimum or unplanned conditions (manufacturing or usage) or when failure can cause significant damage [51, 59].

### 3.3.2 Geometric and mechanical tolerances

The tolerances on diameters and on the thickness of the centre and edges are comparable to general precision manufacturing, typically h6 to h11. When the edge of the window is not fitted and/or it is not a sealing surface the size tolerance is in the 0.1-0.01 mm range. The tolerance on the thickness of the optical access has importance for lenses but for windows it is not crucial. Similarly, the usual parallelism requirements are on the fine side but are comparable but to the ones used in pressure vessel manufacturing. However, the surface roughness values are in a couple of order less than the typical values for precision manufacturing technologies for metals. Moreover, the quality of the finish is further described by the scratch and dig number. A usual scratch/dig specification consists of two numbers e.g. 80/50. The first number indicates the maximum size of cracks (scratches) on the surface of the optical element. The second number describes the maximus size of round-shaped imperfections: digs and pits [60, 61].

Guidelines are given in Table 3 for selecting optical and mechanical properties for sight window applications.

### 3.3.3 Deflection and stress

Equations relating deflection to the applied pressure difference can be found in the literature for a number of shapes and support modes [62, 63]. In this work only the details of relations for the plane-parallel circular window shape are shown.

**Table 2, Classical mechanics of plane-parallel circular elements**

| Non supported case | | Supported case | |
|---|---|---|---|
| 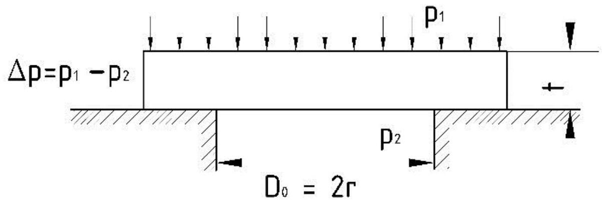  | | 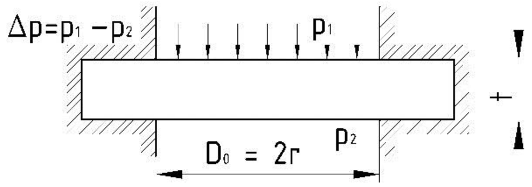  | |
| $\delta = \frac{3(3+\mu)}{8}\frac{\Delta p r^2}{t^2} = K_w \frac{\Delta p r^2}{t^2}$ | **( 3)** | $\delta = \frac{3}{4}\frac{\Delta p r^2}{t^2} = K_w \frac{\Delta p r^2}{t^2}$ | **( 4)** |
| $K_w$=0.125 | **( 5)** | $K_w$=0.75 | **( 6)** |
| $x = \frac{3}{16}(-\mu^2 - 4\mu + 5)\frac{\Delta p r^4}{E t^3} = K_x \frac{\Delta p r^4}{E t^3}$ | **( 7)** | $x = \frac{3}{16}(1-\mu^2)\frac{\Delta p r^4}{E t^3} = K_x \frac{\Delta p r^4}{E t^3}$ | **( 8)** |
| $K_x$=0.96 | **( 9)** | $K_x$=0.17 | **( 10)** |

$K_w$ is a generalised constant suggested by textbooks [51, 52, 59]. In these works, $K_w$ is choosen conservatively to cover a wide range of optical materials. This conservative method was chosen in this study to make a suggestion for values of $K_x$. In the rest of the equations, ( 3)-( 10) $\delta$ is the stress; $\mu$ is the Poisson ratio; $\Delta p$ is the pressure differential; $r$ is the radius which is half of the aperture or diameter $D_0$; $x$ is the defelction; $t$ is the thickness of the optical element; $E$ is Young's modulus. If the the stress equations are rearranged and the safety factor, the diameter and design stress are inserted, then the minimum required thickness of the optical element can be calculated.

$$t_{min} = \left(\frac{1}{2}D_o\right)\left[\frac{K_w\, SF_\delta\, \Delta p}{\delta_{des}}\right]^{1/2} \qquad \textbf{( 11)}$$

where, $t_{min}$ is the minimum thickness of the circular optical element; $D_0$ is the diameter of the aperture; $SF_\delta$ is the safety factor; $\Delta p$ is the applied pressure difference on the optical element; $\sigma_{des}$ is the allowable design stress. Using Equations ( 7) and ( 8), the deflection can be calculated or the rearranged version with the maximum allowable deflection can be used to find the minimum required thickness:

$$t_{min} = \left[\frac{SF_x\, K_x\, \Delta p\, D_0^4}{16\, E\, x_{max}}\right]^{\frac{1}{3}} \qquad \textbf{( 12)}$$

where $SF_x$ is the safety factor. In general, as $SF_\delta$ is associated with complete breakdown and failure and $SF_x$ has an effect on only the quality of the image produced by the optical element. $SF_x$ can have a significantly lower value than the $SF_\delta$. Equation ( 12) provides results for a simple case of a mechanical load. When, there is a combined load from thermal and mechanical loads, the deflection needs to be calculated using Finite Element Analysis (FEA). The result of the simulation can be used to calculate the outer radius ($R$) of the window that can be turned into a divergent meniscus lens (assuming the same deflection on both sides of the window):

$$R = \frac{x^2 + D_0^2}{8x} \qquad \textbf{( 13)}$$

Then with the known thickness the lens power ($P_{lens}$) can be calculated:

$$P_{lens} = (n-1)\frac{-t}{R^2 - Rt} \tag{14}$$

The maximum deflection of a window is a function of allowable image distortion. In an optical system with lens and sensor, the lens focusing error usually gives the tolerance in dioptres. It is hard to find tolerances published, but as a rule of thumb some values are summarised in Table 3, [64-67].

Equations of stress, deflection and power calculation for rectangular, plan parallel windows can be found in [68].

### 3.3.4 Failure estimation by statistical tool

It is a common practice to implement Weibull statistics to estimate the probability of failure ($P_f$ ) when a given $\sigma$ load is applied on a brittle material.

$$P_f = 1 - \exp\left[-\left(\frac{\sigma}{\sigma_0}\right)^m\right] \tag{15}$$

where $m$ is a constant describing the variability in strength; their values having been experimentally determined and published. $\sigma_0$ is a stress level at which 63% of the samples fail, $m$ is the so called Weibull modulus and indicates the scatter of fracture stress around $\sigma_0$ [51, 69-72]. The acceptable values can differ significantly and they should be determined for each application individually. Some suggested examples: for a cheap easily replaceable cutting tool - $10^{-2}$; for an expensive part that upon failure can cause serious damage – $10^{-4}$; when personal injury is at risk – $10^{-6}$; when the outcome of a failure could be fatal then $10^{-8}$.

## 3.4 Optical performance

### 3.4.1 Birefringence and maximum optical path difference (OPD)

It is usual for most practical optical materials to have two indices of refractions. Their refractive index is a function of the propagation-direction and polarisation of the incident electro-magnetic wave. Furthermore, it is a function of the mechanical stress in the medium. Optical substances having this property are called birefringent materials [73]. The level of birefringence is expressed as a difference in the optical path of two perpendicular states of the polarised wave. This inequality in distance is called the OPD and it is measured in nanometres. The OPD has been previously investigated for plane-parallel circular plates with a pressure differential applied on them; Sparks et al. [74] derived an approximate relation:

$$\mathrm{OPD} = 8.89\times10^{-3}(n-1)\frac{\Delta p^2 D^6}{E^2 t^5} \tag{16}$$

where, $\mathrm{OPD}$ is the optical path difference; $n$ is the refractive index of the material; $\Delta p$ is the pressure difference applied across the planes of the optical element; $D$ is the aperture, the unsupported diameter of the optical element; $E$ is Young's modulus of the medium; and $t$ is the thickness of the window. This OPD caused by an applied stress called the stress birefringence. It is measured as OPD per unit travel path; its unit is nm/cm. The details of the maximum allowable tolerances on birefringence for some applications are given in ISO 10110-8 [61] and Kimmel and Parks [75]; a summary is presented in Table 1. Equation ( 16) can be rearranged to find the minimal required thickness:

$$t_{min\,|ODP\Delta p} = \sqrt[5]{8.89\times10^{-3}(n-1)\frac{\Delta p^2 D^6}{\mathrm{OPD}\cdot E^2}} \tag{17}$$

**Table 3. Sight window properties for different applications**

| Precision | Typical application | Maximum power of a deflected window (dioptre) | Maximum OPD per unit path length (nm/cm) | Parallelism or plane angle (degree) | Flatness ($\lambda$ is the characteristic wavelength) | Surface finish or roughness (nm) | Surface finish quality |
|---|---|---|---|---|---|---|---|
| Extreme | Polarisation and interference instrumentation, deep-space instrumentation | No data | 2 | No data | $\frac{\lambda}{20}$ or better | 0.3 | No data |
| High | Photolithography optics and astronomical telescopes | No data | 5 | 0.001 | $\frac{\lambda}{10}$ | 0.5 | 10/5 |
| Good | Photographic and microscope optics, visual telescope | $10^{-2} - 10^{-6}$ * | 10 | 0.01-0.001 | $\frac{\lambda}{2} - \frac{\lambda}{4}$ | 1 | 40/20-20/10 |
| Semi | Eyepieces, viewfinders, magnifying glasses | $10^{-1}$ | 20 | 0.1-0.01 | $\lambda$ | 2 | 60/40 |
| Commercial | Illumination optics, condenser lenses | No req.** | No req. | 0.1 | No req. - $2\lambda$ | 4 | 80/50 |

*in general it can be said that, tolerance values in the order of $10^{-6}$ or less are likely to be negligible when they are compared to the uncertainty in the focus adjustment of a lens system

** No req.: No requirement

It is important to note that there are always some residual stresses in optical materials, depending on the quality of the manufacturing processes. More details relating the manufacturing process to stress birefringence can be found in the references.

## 3.5 Factors limiting the maximum thickness

- The most obvious limiting factor is the available space the geometric constraints, which depends on the individual design. The different possible mounting methods and previous publications of solutions are introduced in other sections of this work.
- Transmittance change as a function of material thickness [27]. Significant decrease of the transmittance can only occur with large thicknesses, this is not a usual design constraint for high load applications.
- Temperature gradients can cause stress concentration in window materials. For heated or cooled designs this can limit the size of the geometry. Ceramics with larger thermal conductivity coefficients are less sensitive to thermal shock, [76, 77].
- Price: manufacturing and material cost
  As Figure 8 indicates typically there is a thickness range where the price is at its minimum. This is the most commonly made size range($t \leftrightarrow pt; p{\sim}3 \ldots 5$) that is mass produced with a variety of tolerances and finishes. These are usually used in general optics and not adequate for high load applications. To the left from this region ($t \leftrightarrow mt; m{\sim}0.6 \ldots 1.0$) there is an increase in price where the manufacturing becomes more laborious. The relatively thin geometry makes the window fragile and prone to deflection under the manufacturing loads. A further sharp rise expected for thicknesses below $mt$ where extra care is required to provide precision finish. For example, during manufacturing there is a 50% breakage rate for 0.2mm borosilicate glass coverslips. On the right hand side from the flat ($pt \leftrightarrow nt; n{\sim}\text{few hundreds}$) the increase is driven by the cost of material. $nt$ represents

the maximum size that is achievable using the standard or already existing raw material production tooling. Larger geometries can only be made if tooling cost is covered.

Figure 8 only introduces general trends in the price the actual values will differ from geographic region to region, material type, and quantity required.

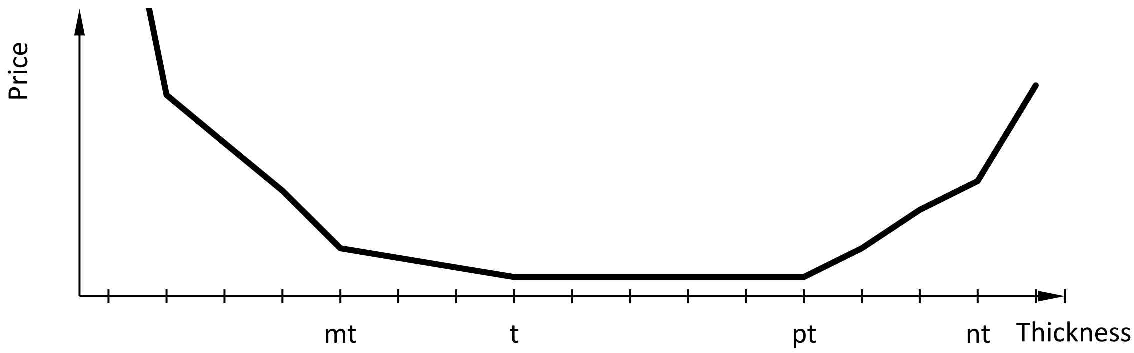


**Figure 8. Approximate cost of manufacturing of disc-shaped windows as function of thickness**

## 3.6 Other design considerations

In this section further design considerations are listed and referenced. They are not of interest to this study, but they can be potentially important for other designs, for instance, in applications where the pressurised chamber is used with high accuracy polarisation or interference instruments or deep space applications.

- Compressive stress caused by sharp edges on the surface of an optical element [78, 79]
- Effect of a temperature gradient on adhesive bonds [52, 80]
- The tensile stress in a brittle material due to a compressive load on its surface [52, 63, 81]
- Focus shift in thick parallel plane optical elements [82]
- Distortion caused by a temperature gradient [71, 83-85]

# 4 Design of an optically accessible pressure chamber

The detailed geometry of the existing combustor is shown in Figure 9. An important feature of it is that the working chamber was constructed from sections. Utilising this property, the reactor's length could be varied to adjust the residence time of the reactants. Different length sections were available to build the reactor. When the reactor was assembled, the sections were sealed by polymer O-rings. As a result of the limited temperature resistance of the stainless steel structure and the high thermal load, the sections had to be individually water-cooled, as in Figure 9.

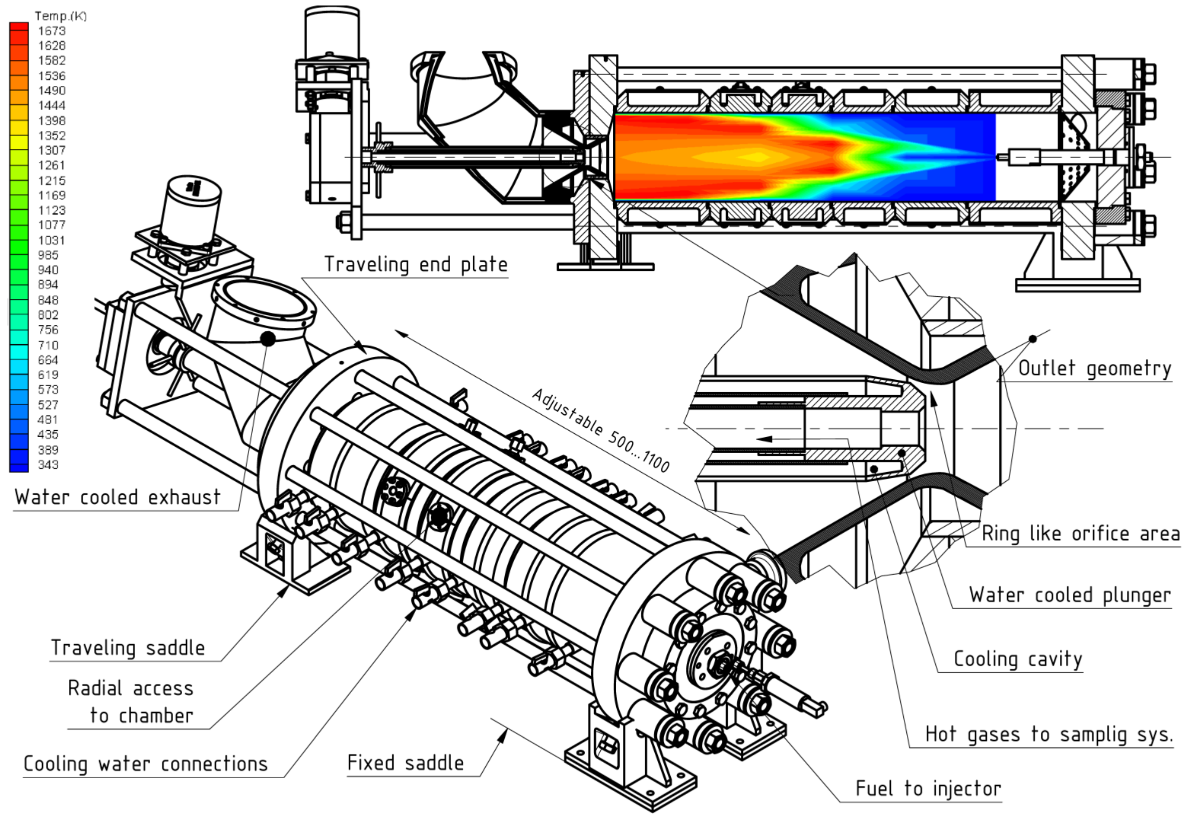


**Figure 9. An isometric and a section view of existing chamber, computational result of in-cylinder temperature distribution shown in the section view. Conditions: diesel fuel; stoichiometric ratio; 6 bar in-reactor pressure.**

## 4.1 Section

### 4.1.1 Design requirements

It was required that the optical section withstand the maximum of 20 bar working pressure at the maximum possible operating temperature and that its geometry would allow it to be connected it to the existing rig. In order to seal the reactor, it was essential to maintain the temperature at an acceptable level in the O-ring grooves. The maximum continuous operating temperature of the Viton O-rings (200 °C) was chosen as a limit on the surfaces that were in contact with the rings. The system could provide a maximum cooling flow rate of 10 litres per minute for the new optical section. The highest allowed inflow cooling temperature was 70 °C. The estimation of the heat flux coming from the combustion to the section was based on a number of test results where an in-chamber, single-point gas temperature measurement was taken. An example of these results is shown in Figure 10. The results of computational work on combustion and in-chamber conditions by Demosthenous and Crookes [10] were used as input boundary conditions for the analysis, Figure 9. It was also a requirement that the windows could be easily changed to metal blanks for heating up or non-optical tests.

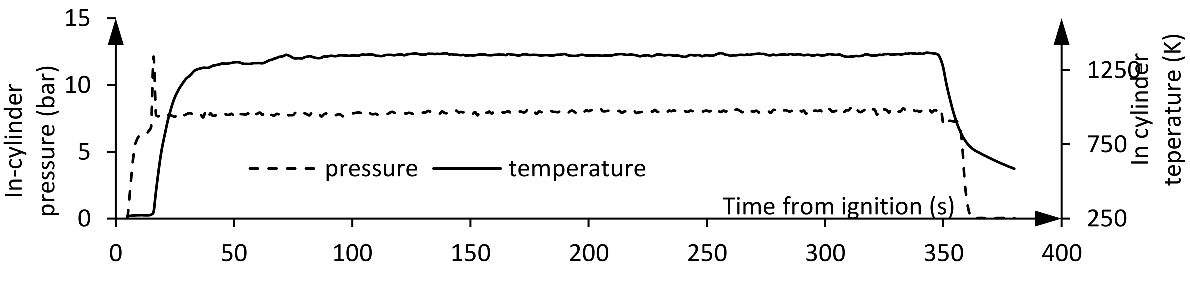


**Figure 10. Typical test results of the existing combustion chamber; the time of ignition is indicated by the rapid increase in temperature and a pressure peak at around 10s after ignition**

It was an underlying requirement that the new apparatus would allow investigation with a Phantom 4.3 high speed camera, a TSI Particle image velocimetry system (laser: dual 50 mJ/pulse, NewWave Gemini Nd:YAG; sensor: PowerView 4MP) and a FLIR Titanium 560M infrared (IR) camera.

### 4.1.2 Material choice

As shown in Figure 12, the resultant optical section is a complex shape, featuring fine finished surfaces for sealing purposes. It is thus that the material of the section body needed to have adequate strength to withstand the pressure load at high temperatures. It also needed to be suitable for precision subtractive and additive manufacturing. Moreover, due to the corrosive products forming inside the chamber and the constant presence of cooling water, the material was required to have some corrosion-resistant properties. A detailed list of possible materials can be found in EN134453 [86]. The aforementioned requirements suggested using an austenitic stainless steel grade. After considering the cost, the corrosion resistance and manufacturability grade 304 (1.403) was chosen. It is easily available, with well-documented data on its mechanical properties at elevated temperatures showing the tensile stress for the materials that were used to construct the optical combustor, Figure 11.

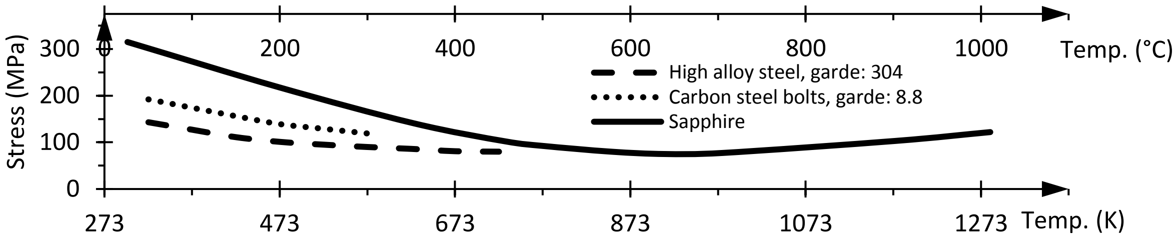


**Figure 11. Permissible design stresses of some selected materials as function of temperature [37, 56].**

### 4.1.3 Design of required geometry and validation

This structure of the overall design defined some underlying properties of the optical access. It was the obvious choice that the optical access should be constructed on a section which has similar dimensions and had the same sealing method. Given the nature of the laser-radiation-based measurement method, a three-access point – in a T-like configuration – was required. A detailed review of optical measurements can be found in the books by Zhao [12, 13]; see details in Figure 12. This three-access point design was satisfactory for the high speed and IR camera setup.

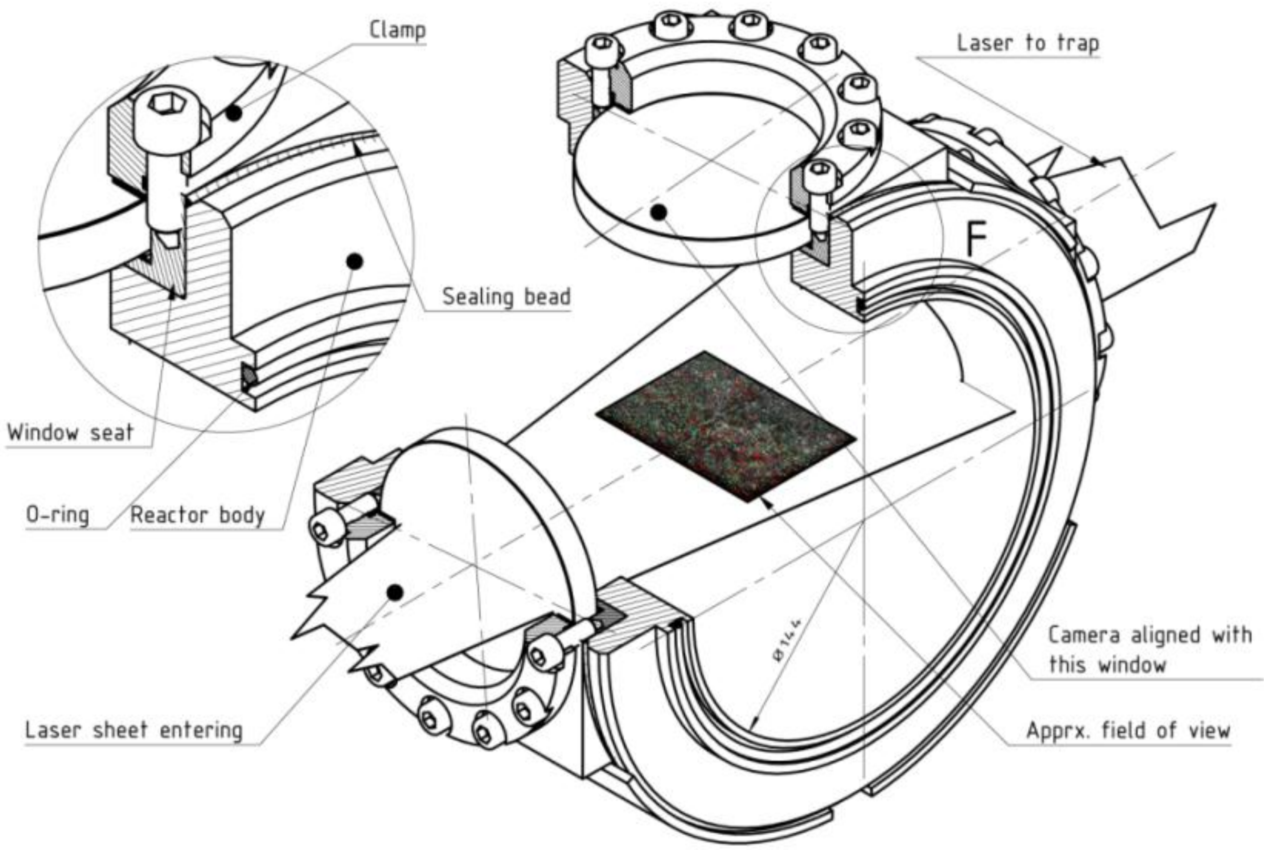


**Figure 12. The final design of the optical section. The laser sheet entering and leaving the chamber is also indicated.**

It can be seen that cooling was essential for the operation of this reactor. Insufficient cooling would result in a rapid increase of temperature in the body and in the window (or blank). With the increased temperature the polymer seals would quickly fail. Therefore, the geometry of the body with window seats had to provide enough surface area for the coolant and allow sufficient volume flow. Assuming the largest heat flux and inflow cooling temperature, a number of simulations were carried out to plot the O-ring groove temperature curve against the coolant flow rate. It was found that having at least 5.5 litres per minute coolant flow rate on the designed geometry could keep the O-ring groove temperature at an acceptable level. The 5.5 litres per minute minimum cooling flow requirement is below the 10 litres per minute maximum performance, therefore the given cooling system was found to be sufficient.

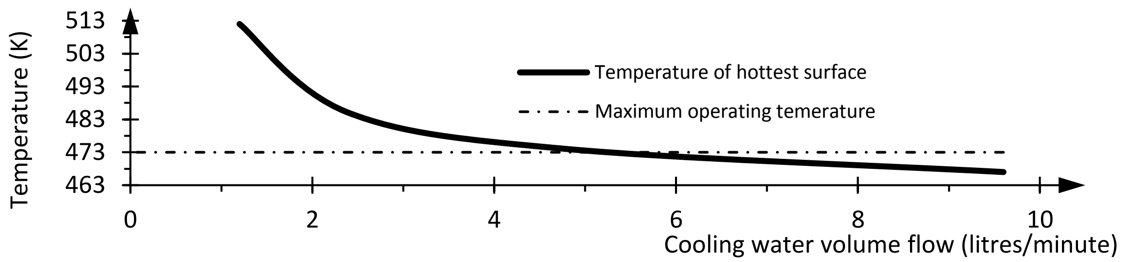


**Figure 13. The O-ring groove temperature as the function of the coolant volume flow (value was taken from the corner point of the hottest possible cross section, as indicated in Figure 15b).**

The length of the section was chosen to be the same as that of the longest existing section. The thickness of the optical section was based on the existing design. Polymer O-rings were used to seal between the sections, the design and manufacturing were according to BS ISO 3601 [87]. With the given length, a circular window type was selected for easier machining and the geometrically maximum possible diameter, 82 mm, was chosen to be evaluated. FEA was carried out to determine the stress arising from thermal loads and applied pressure. As is indicated in Figure 14, the highest stresses are in the O-ring grooves and in the openings. The grooves had high stresses on their contact surfaces because of the large axial force pressing the sections together against the pressure. In the case of the openings the high stress rate can be explained by the reduced material volume, i.e. reduced inertia [88].

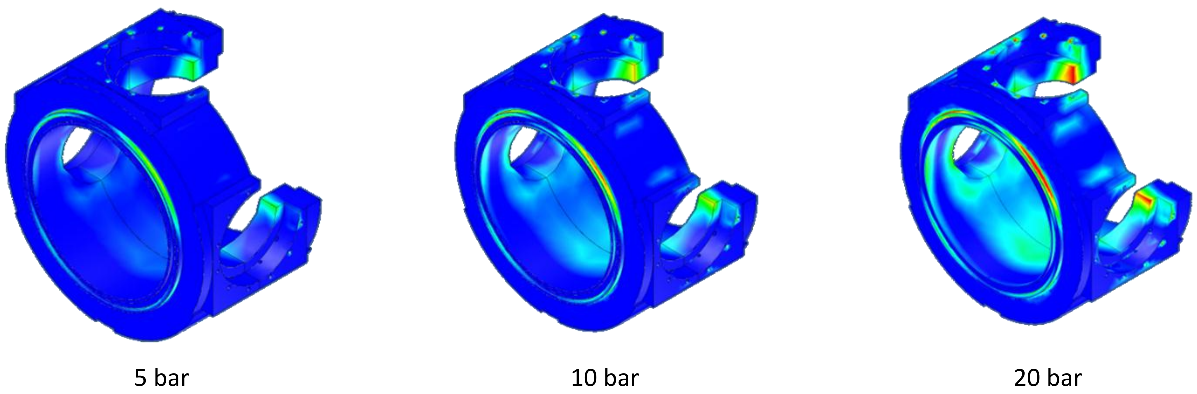


**Figure 14. Stress distribution as a function of chamber pressure**

The inner diameter of the optical section is 144 mm; the outer diameter is constrained by the support rods, as seen in Figure 9. As the radial space was limited, the best design solution would have been to place the optical element inside the shell – but with the given casted base, this was not achievable. Therefore, the second best option – with an eye to optimising storage space – was to have a free sitting clamp; this setup is shown in Figure 12. The detailed section-view shows the window kept in place by the circular clamp. The clamps were fixed and positioned by 12 M6 socket-head bolts to the window seats. The window seats were welded all around to the base chamber or reactor body; the beads sealed the seats and kept them in place. The window to seat-sealing surfaces were precision-manufactured, as suggested in PD5550:2009 Table 3.8-3 [89]. With the aid of the measurements and computational results, further analysis was carried out to estimate the working temperature of the section and optical elements. The temperature distribution of the cross-sections is shown in Figure 15.

## 4.2 Window

### 4.2.1 Design requirements

The main purpose of the window is to provide a transparent barrier between the combustion and instrumentation. An underlying requirement was to allow use of three different sensors (cameras) with differing spectral responses. Wavelengths of interest are particulate imaging velocimetry (around 532 nm), high speed camera (visible spectra) and IR camera (3 to 5 micron); the responsivity curves are shown in Figure 2. As the wavelength of the laser is in the visible range, there were two bands of electromagnetic radiation that needed to be considered – 380-985 and 2800-5200 nm. In these regions, the minimum of 80% transmittance was required. The tolerance on the OPD had to be kept in the photographic range: 10 nm/cm. As the three sensors were robust and the measurements by them were not overly sensitive, the maximum allowed lens power of the distorted window was $10^{-6}$ dioptre. The maximum expected pressure difference on the optical element was 20 bar. The required safety factor was required to be four for stresses arising from mechanical and thermal loads, with a maximum probability failure of $10^{-4}$. The technological considerations and tolerances were chosen to fit laser and the precision measurements requirements. The level of precision was selected to be good according to Table 3. Finally, the operating temperature of the window had to stay under the maximum permitted level.

### 4.2.2 Material choice for optical element

The spectral requirement is shown in Figure 2 along with the transmittance curves. The ideal design solution was to select only one material type to cover the required wavelength ranges. It can be seen that the two possible material types that cover the needed large range of EM wavelengths are sapphire and magnesium fluoride. The thermal analysis of the optical section indicated that the steel blanks and windows would need cooling to survive. The calculations and simulations were carried out for both materials. It was found that $MgF_2$ can be a valid option for low-temperature and low-humidity environments. Extra caution is required when a temperature gradient is applied on the $MgF_2$ material, as its high expansion coefficient and middle-range conductivity combined with low strength makes it sensitive to thermal shock. It is also suggested by manufacturers that $MgF_2$ can react with high temperature steam similar to the one that can be found in the HPC as a combustion product. Therefore, sapphire was, instead, chosen as material for the windows as it combines good transmittance in all the required wavelength bands as well as having good thermo-mechanical strength.

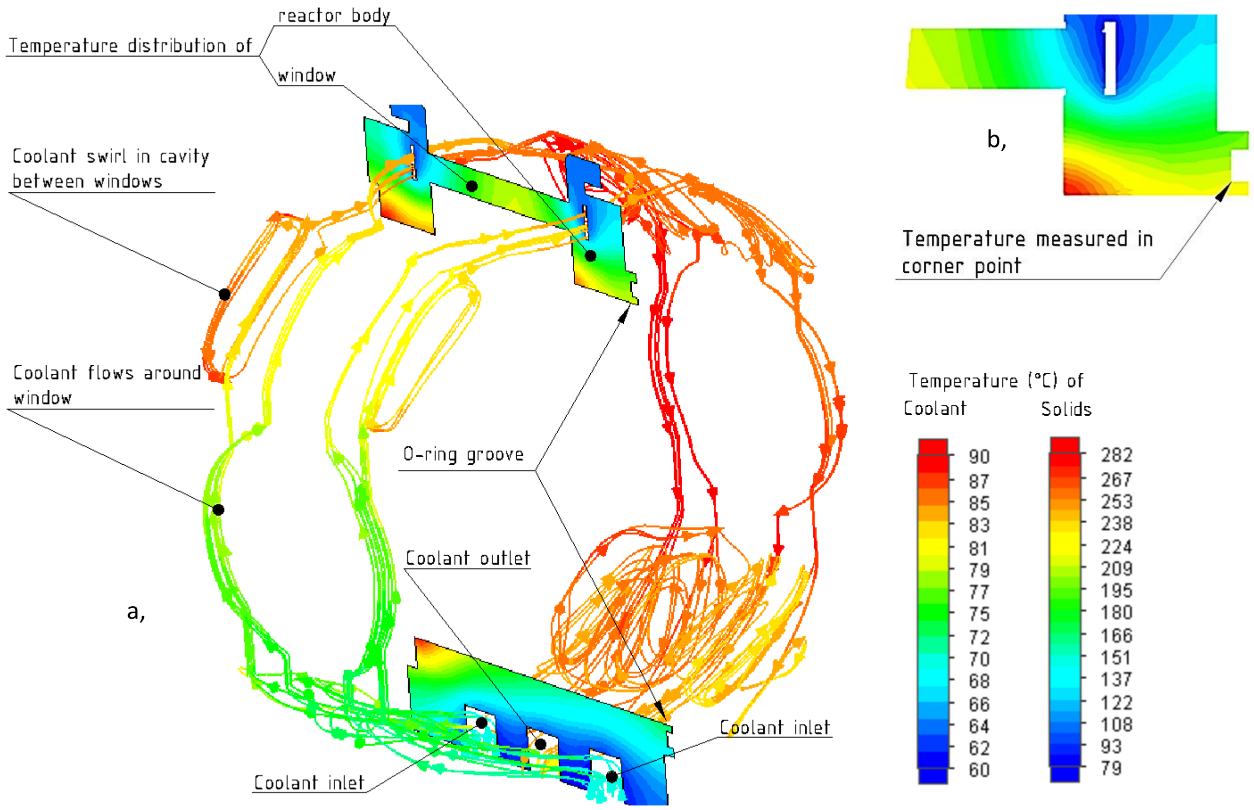


**Figure 15. a) An isometric view of the flow of cooling water, its temperature change and the temperature distribution of a cross section of the reactor. b) Temperature distribution around the O-ring groove.**

### 4.2.3 Design of required geometry and validation

The diameter of the window was determined by the maximum available space in the optical section. The maximum possible diameter was found to be 82 mm. Previous experience showed that a width of 9 mm minimum contact surface is required to provide an adequate sealing performance. The 9 mm wide contact ring also ensured an acceptable level of compressive stress in the window and provided large enough heat transfer surface for the metal blanks. This geometric design resulted in a 64 mm aperture. The thickness of the window was estimated by using the equations and relations that were explained earlier in this paper, and then validated by FEA. The minimum thickness was calculated for two requirements: maximum allowable stress and OPD. Substituting values to Equations ( 11) and ( 17) the thickness value results were 5.88 and 0.07 mm respectively.

$$t_{min\,|\delta} = \left(\frac{1}{2}D_o\right)\left[\frac{K_w\, SF_\delta\, \Delta p}{\delta_{des}}\right]^{1/2} = \left(\frac{1}{2}64\text{mm}\right)\left[\frac{0.75\cdot\ 4\cdot\ 2\text{MPa}}{178\text{MPa}}\right]^{1/2} = 5.88\text{mm} \quad (18)$$

$$t_{min|ODP\Delta p} = \sqrt[5]{8.89\cdot 10^{-3}(n-1)\frac{\Delta p^2 D^6}{\text{OPD}\cdot E^2}} = \sqrt[5]{8.89\cdot 10^{-3}(1.76-1)\frac{(2\text{MPa})^2\cdot(64\text{mm})^6}{10\frac{\text{nm}}{\text{cm}}\cdot(345\text{GPa})^2}} = 0.07\text{mm} \quad (19)$$

The results of the estimation indicated that, with the given loads and geometry, the required optical performance was easily achievable. Then, the window deflection was calculated using FEA for the highest thermal and mechanical loads. The stress and deflection results were substituted in Equations ( 13), ( 14) and ( 15) in order to check the design for failure probability and image distortion. Equations ( 13) and ( 14) combined together gives the power of a distorted window as function of refractive index, aperture and deflection.

$$P_{lens} = \frac{64(n-1)tx_{(t)}^2}{\left(D_0^2 + x_{(t)}^2\right)\left(D_0^2 + x_{(t)}\left(x_{(t)} - 8t\right)\right)} \qquad (20)$$

The power as function of window thickness for the given geometry is shown in Figure 16.

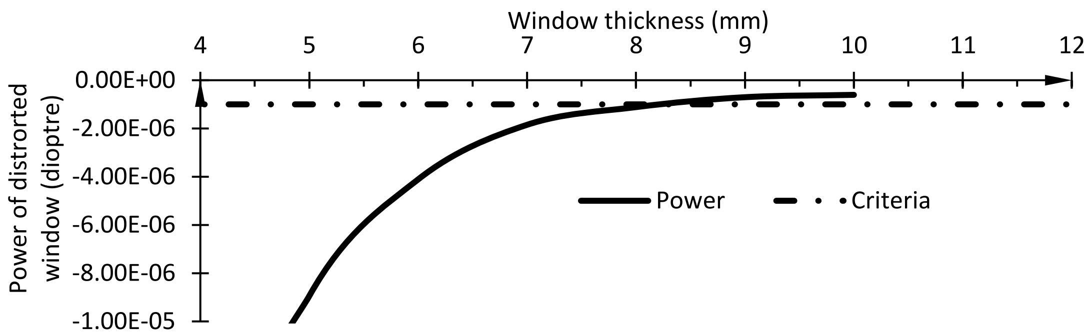


**Figure 16. Power of distortion vs window thickness**

It was found that the limiting factors were the probability failure and deflection. Based, on the curve above and financial consideration the thickness was chosen to be 10mm. Using FEA, the maximum stress was found to be 42.8MPa, with this level of stress:

$$P_f = 1 - \exp\left[-\left(\frac{\sigma}{\sigma_0}\right)^m\right] = 1 - \exp\left[-\left(\frac{42.8\text{MPa}}{485\text{MPa}}\right)^5\right] = 5.35 \cdot 10^{-6} \qquad (21)$$

However, there is a high inaccuracy in the result of probability failure and therefore the result is only a guideline. The value of $\sigma_0$ is function of a number of variables, one of the most important ones is temperature. There is a no data available for $\sigma_0$ in the literature for elevated temperatures.

# 5 Results and Conclusion

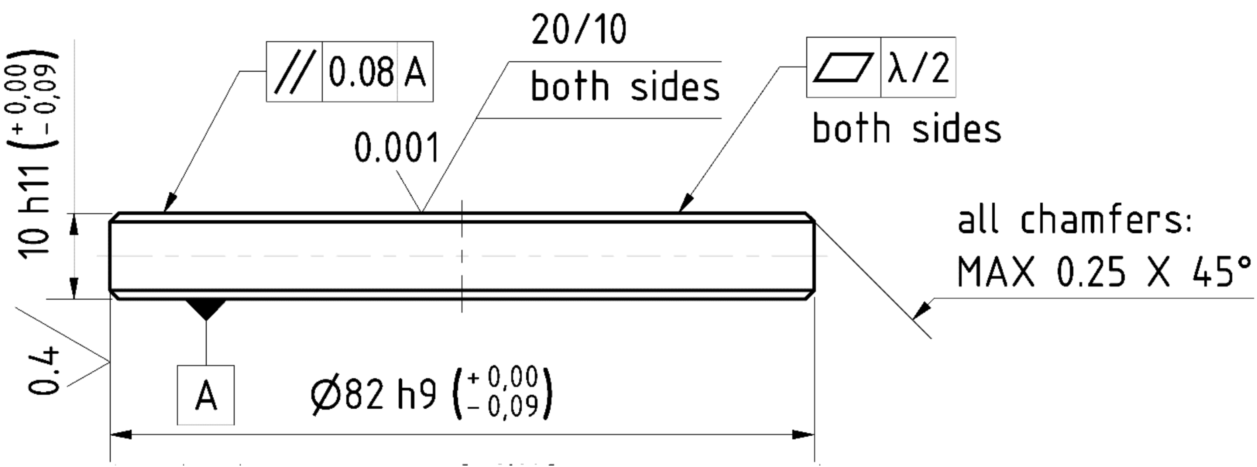


**Figure 17. Side view: final sapphire sight window design, where $\lambda = 532\text{nm}$**

This work has investigated the design of pressure vessels equipped with optical access. A significant number of data sources were surveyed to produce a comprehensive review of the most related optical, thermal and mechanical properties for some optical materials. The database was presented in a way that allows for a convenient and direct comparison. The little design data that was available on the topic in the literature was presented, while also considering practical, mechanical and optical design considerations. The aspects of the design for optical performance were described in-depth, with additions to the already published equations and relations. The utilisation of this database allowed for the design process of a pressure chamber, with optical element under high mechanical and thermal load, to be demonstrated, where, the required experimental rig needed to support research activity for a range of optical instrumentation. Figure 18 indicates the results gained from the working optical section.

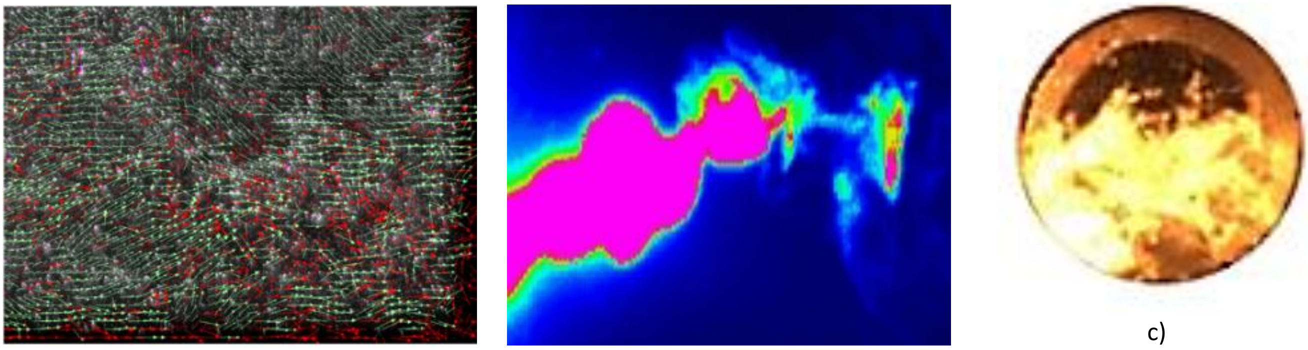

a) b) c)

**Figure 18. Results from the optical HPC: a) PIV vector field of the flowing air fuel mixture. b) IR radiation image recorded from a hydrocarbon flame. c) A still image from high speed video.**


# 6 Acknowledgement

The modelling and simulations were carried out with SolidWorks under an academic licence. This research project was supported by the Central Research Fund of University of London. The authors are grateful for the countless advice and information on manufacturing provided by Mr Anthony Otten and Mr Vince Ford.


# 7 References


[1] L. Kosnik, The potential for small scale hydropower development in the US, Energy Policy 38(10) (2010) 5512-5519.

[2] H. Siebert, The Problem, Economics of the Environment, Springer Berlin Heidelberg2008, pp. 3-6.

[3] N. Stern, The Economics of Climate Change, The Stern Review, Cambridge University Press2007.

[4] T. Korakianitis, S. Imran, D.R. Emberson, A.M. Namasivayam, R.J. Crookes, Internal Combustion Engine Performance and Emissions Aspects When Fueled by Conventional and Sustainable Fuels, Handbook of Clean Energy Systems.

[5] M. Höök, X. Tang, Depletion of fossil fuels and anthropogenic climate change - A review, Energy Policy 52(0) (2013) 797-809.

[6] B. Ihracska, T. Korakianitis, P. Ruiz, D.R. Emberson, R.J. Crookes, A. Diez, D. Wen, Assessment of elliptic flame front propagation characteristics of iso-octane, gasoline, M85 and E85 in an optical engine, Combustion and Flame 161(3) (2014) 696-710.

[7] B. Ihracska, D. Wen, S. Imran, D.R. Emberson, L. Maria Ruiz, R.J. Crookes, T. Korakianitis, Assessment of elliptic flame front propagation characteristics of hydrogen in an optically accessible spark ignition engine, International Journal of Hydrogen Energy 38(35) (2013) 15452-15468.

[8] S. Imran, D. Emberson, A. Diez, D. Wen, R. Crookes, T. Korakianitis, Natural gas fueled compression ignition engine performance and emissions maps with diesel and RME pilot fuels, Applied Energy 124 (2014) 354-365.

[9] R.J. Crookes, Soot Formation and Oxidation at High Pressure in a Confined Spray Flame, Combustion Science and Technology 178(8) (2006) 1491-1510.

[10] A. Demosthenous, Soot formation and oxidation in a high-pressure spray flame, Queen Mary, University of London, 2005.

[11] M.A.A. Nazha, R.J. Crookes, Design and Operation of a High-Pressure Combustion System for Study of Soot Formation, SAE International, 1992.

[12] H. Zhao, N. Ladommatos, Engine Combustion Instrumentation and Diagnostics, SAE International2001.

[13] H. Zhao, Laser Diagnostics and Optical Measurement Techniques in Internal Combustion Engines, 2012.

[14] D. Emberson, B. Ihracska, S. Imran, A. Diez, Optical characterization of Diesel and water emulsion fuel injection sprays using shadowgraphy, Fuel 172 (2016) 253-262.

[15] J. Mackerle, Finite elements in the analysis of pressure vessels and piping, an addendum: A bibliography (2001–2004), International Journal of Pressure Vessels and Piping 82(7) (2005) 571-592.

[16] H. Mayer, H. Stark, S. Ambrose, Review of fatigue design procedures for pressure vessels, International journal of pressure vessels and piping 77(13) (2000) 775-781.

[17] R. Preiss, Design-by-analysis of a chemical reactor's head under sustained and thermal loads, International journal of pressure vessels and piping 77(6) (2000) 277-288.

[18] M. Staat, M. Heitzer, H. Lang, K. Wirtz, Direct finite element route for design-by-analysis of pressure components, International Journal of Pressure Vessels and Piping 82(1) (2005) 61-67.

[19] M.J. Hyder, M. Asif, Optimization of location and size of opening in a pressure vessel cylinder using ANSYS, Engineering Failure Analysis 15(1-2) (2008) 1-19.

[20] S. Chattopadhyay, Pressure Vessels: Design and Practice, CRC Press LLC2005.

[21] J. Spence, D.H. Nash, Milestones in pressure vessel technology, International Journal of Pressure Vessels and Piping 81(2) (2004) 89-118.

[22] D. Nash, M. Abid, Combined external load tests for standard and compact flanges, International journal of pressure vessels and piping 77(13) (2000) 799-806.

[23] H. Darijani, M.H. Kargarnovin, R. Naghdabadi, Design of thick-walled cylindrical vessels under internal pressure based on elasto-plastic approach, Materials & Design 30(9) (2009) 3537-3544.

[24] S.M. Hosseini, Coupled thermoelasticity and second sound in finite length functionally graded thick hollow cylinders (without energy dissipation), Materials & Design 30(6) (2009) 2011-2023.

[25] H.R. Zare, H. Darijani, A novel autofrettage method for strengthening and design of thick-walled cylinders, Materials & Design 105 (2016) 366-374.

[26] C. Nadarajah, L. Foo, Finite element study of keyed backing ring design for floating head, International journal of pressure vessels and piping 75(6) (1998) 521-526.

[27] Schott, TIE-35: Transmittance of optical glass, 2005.
[28] Schott, TIE-31: Mechanical and Thermal Properties of Optical Glass, 2004.
[29] K.B. Doyle, M.A. Kahan, Design strength of optical glass, Proceedings of SPIE 5176 Optomechanics (2003) 14-25.
[30] Hoya, Optical Glass: Specifications.
[31] Schott, Technical Glasses, Physical and technical properties, 2010.
[32] ISO, Optics and photonics -- Specification of raw optical glass, 2010.
[33] M.J. Weber, Handbook of Optical Materials, CRC Press2002.
[34] A.K. Koenig Spilman, Stress-Engineered Optical Elements, School of Engineering and Applied Sciences, University of Rochester, 2007.
[35] C.A. Klein, Characteristic strength, Weibull modulus, and failure probability of fused silica glass, Optical Engineering 48(11) (2009) 113401-113401-10.
[36] J. Detrio, D. Iden, F. Orazio, S. Goodrich, G. Shaughnessy, Experimental validation of the Weibull area-scaling principle, Proc. 12th DoD Electromagnetic Windows Symp, 2008, p. 434.
[37] O.V. Voloshyn, L.A. Lytvynov, E.V. Slyunin, Potentialities for sapphire strength enhancement, Functional Materials 14(4) (2007) 569-569.
[38] D.A. Ditmars, S. Ishihara, S.S. Chang, G. Bernstein, E.D. West, Enthalpy and Heat-Capacity Standard Reference Material: Synthetic Sapphire Al2O3 From 10 to 2250 K, JOURNAL OF RESEARCH of the National Bureau of Standards 87(2) (1982) 159-159.
[39] L.S. Combes, S.S. Ballard, K.A. McCarthy, Mechanical and Thermal Properties of Certain Optical Crystalline Materials, J. Opt. Soc. Am. 41(4) (1951) 215-221.
[40] D.C. Harris, High-temperature strength of sapphire, International Symposium on Optical Science and Technology, International Society for Optics and Photonics, 2000, pp. 25-36.
[41] F. Schmid, D.C. Harris, Effects of crystal orientation and temperature on the strength of sapphire, Journal of the American Ceramic Society 81(4) (1998) 885-893.
[42] G. Wang, H. Zuo, H. Zhang, Q. Wu, M. Zhang, X. He, Z. Hu, L. Zhu, Preparation, quality characterization, service performance evaluation and its modification of sapphire crystal for optical window and dome application, Materials & Design 31(2) (2010) 706-711.
[43] W. Wunderlich, H. Awaji, Molecular dynamics — simulations of the fracture toughness of sapphire, Materials & Design 22(1) (2001) 53-59.
[44] H.W. Icenogle, B.C. Platt, W.L. Wolfe, Refractive indexes and temperature coefficients of germanium and silicon, Applied Optics 15(10) (1976) 2348-2351.
[45] A. Duncanson, R.W.H. Stevenson, Some Properties of Magnesium Fluoride crystallized from the Melt, Proceedings of the Physical Society 72(6) (1958) 1001-1001.
[46] P. Laporte, J.L. Subtil, M. Courbon, M. Bon, L. Vincent, Vacuum-ultraviolet refractive index of LiF and MgF2 in the temperature range 80--300 K, Journal of the Optical Society of America 73(8) (1983) 1062-1069.
[47] A. Diez, R.J. Crookes, T. Løvås, Experimental studies of autoignition and soot formation of diesel surrogate fuels, Proceedings of the Institution of Mechanical Engineers, Part D: Journal of Automobile Engineering 227(5) (2013) 656-664.
[48] J.G. Williams, R.E. Anley, D.H. Nash, T.G.F. Gray, Analysis of externally loaded bolted joints: Analytical, computational and experimental study, International Journal of Pressure Vessels and Piping 86(7) (2009) 420-427.
[49] A.-H. Bouzid, Comparative study of bolt spacing formulas used in bolted joint designs, International Journal of Pressure Vessels and Piping 120-121 (2014) 47-54.
[50] T.J. Manuccia, J.R. Peele, C.E. Geosling, High temperature ultrahigh vacuum infrared window seal, Review of Scientific Instruments 52(12) (1981) 1857-1859.
[51] P.R. Yoder Jr, Mounting Optics in Optical Instruments, SPIE Press2008.
[52] P.R. Yoder Jr, Opto-mechanical systems design, SPIE Press2006.
[53] G. Dunn, J. Stachiw, Acrylic windows for underwater structures, Underwater Photo Optics I, International Society for Optics and Photonics, 1966, pp. 157-168.
[54] G.M. Dunn, J.D. Stachiw, Acrylic Windows For Underwater Structures, Proccedings of SPIE 0007 (1966) 157-168.
[55] M. Abid, D.H. Nash, A parametric study of metal-to-metal contact flanges with optimised geometry for safe stress and no-leak conditions, International Journal of Pressure Vessels and Piping 81(1) (2004) 67-74.
[56] BS EN, 13445-3: Unfired pressure vessels - Part3: Design, 2009.
[57] ASME, ASME Boiler and Pressure Vessel Code, Section VIII, Division 3, New York, 2004.
[58] A.T. Diamantoudis, T. Kermanidis, Design by analysis versus design by formula of high strength steel pressure vessels: a comparative study, International Journal of Pressure Vessels and Piping 82(1) (2005) 43-50.
[59] D.C. Harris, Materials for infrared windows and domes: properties and performance, SPIE press1999.
[60] M. Specifications, Optical Components for Fire Control Instruments; Genereal Specification Governing the Manufacture, Assembly, 1963.
[61] ISO, Optics and photonics -- Preparation of drawings for optical elements and systems -- Part 8: Surface texture; roughness and waviness, 2010.
[62] R.J. Roark, Formulas for Stress and Strain, McGraw-Hill Book Co Inc., New York, 1954.
[63] W.C. Young, R.G. Budynas, Roark's formulas for stress and strain, McGraw-Hill New York2002.
[64] R.E. Fischer, B. Tadic-Galeb, P.R. Yoder, R. Galeb, Optical system design, McGraw Hill New York2000.
[65] D.R. Hearn, Vacuum window optical power induced by temperature gradients, SPIE's International Symposium on Optical Science, Engineering, and Instrumentation, International Society for Optics and Photonics, 1999, pp. 297-308.
[66] R. Kingslake, R.B. Johnson, Lens design fundamentals, academic press2009.
[67] C.A. Klein, J. Pappis, ZnS, ZnSe, and ZnS/ZnSe windows: their impact on FLIR system performance, Optical Engineering 25(4) (1986) 254519-254519-.
[68] B. Ihracska, Combustion of Alternative Fuels: Opto-Mechanical Design and Optical Investigation, Queen Mary University of London, 2016.
[69] M.F. Ashby, Materials selection in mechanical design, Butterworth-Heinemann, Oxford, 2005.

[70] K.B. Doyle, M.A. Kahan, Design strength of optical glass, Optical Science and Technology, SPIE's 48th Annual Meeting, International Society for Optics and Photonics, 2003, pp. 14-25.
[71] D. Vukobratovich, Optomechanical Design Principles, CRC Press LLC1999.
[72] J. Wannenburg, G.C. Klintworth, A.D. Raath, The use of probability theory in fracture mechanics—A case study, International Journal of Pressure Vessels and Piping 50(1–3) (1992) 255-272.
[73] J. Daintith, Oxford dictionary of physics, Oxford University Press Oxford, 2005.
[74] M. Sparks, M. Cottis, Pressure-induced optical distortion in laser windows, Journal of Applied Physics 44(2) (1973) 787-794.
[75] R.K. Kimmel, R.E. Parks, ISO 10110 Optics and Optical Instruments: Preparation of Drawings for Optical Elements and Systems: a User's Guide, Optical Society of America2002.
[76] D. Hasselman, Unified theory of thermal shock fracture initiation and crack propagation in brittle ceramics, Journal of the American Ceramic society 52(11) (1969) 600-604.
[77] D. Li, W. Li, W. Zhang, D. Fang, Thermal shock resistance of ultra-high temperature ceramics including the effects of thermal environment and external constraints, Materials & Design 37 (2012) 211-214.
[78] R. Delgado, M. Hallinan, ‘Mounting of Lens Elements, Opt. Eng 14 (1975) 11.
[79] P.R. Yoder Jr, Parametric investigations of mounting-induced axial contact stresses in individual lens elements, SPIE's 1993 International Symposium on Optics, Imaging, and Instrumentation, International Society for Optics and Photonics, 1993, pp. 8-20.
[80] W. Chen, C. Nelson, Thermal stress in bonded joints, IBM Journal of Research and Development 23(2) (1979) 179-188.
[81] S. Timoshenko, J. Goodier, H.N. Abramson, Theory of elasticity, Journal of Applied Mechanics 37 (1970) 888.
[82] J.E. Greivenkamp, Field Guide to Geometrical Optics, Spie Press2004.
[83] W.P. Barnes Jr, Some effects of aerospace thermal environments on high-acuity optical systems, Applied optics 5(5) (1966) 701-711.
[84] M.C. Dudzik, Electro-Optical Systems Design, Analysis, and Testing, SPIE Optical Engineering Press1993.
[85] F. Shahabian, S.M. Hosseini, Stochastic dynamic analysis of a functionally graded thick hollow cylinder with uncertain material properties subjected to shock loading, Materials & Design 31(2) (2010) 894-901.
[86] B. EN, 13445-3: 2009, BSI British Standards. Unfired pressure vessels-Part.
[87] BS ISO, Fluid power systems. O-rings. Inside diameters, cross-sections, tolerances and designation codes, 2012.
[88] S.R. Lin, J.S. Yu, C.S. Chang, Stress analysis of screws in the fuel channel fastener assembly, International Journal of Pressure Vessels and Piping 117-118 (2014) 49-55.
[89] BSI, PD 5500 Specification for unfired fusion welded pressure vessels, 2009.